Applied Surface Science 504 (2020) 144453

Contents lists available at ScienceDirect

Applied Surface Science

journal homepage: www.elsevier.com/locate/apsusc

Full Length Article

Surface modification of CrFeCoNiMo high entropy alloy induced by high-current pulsed electron beam

Peng Lyu[a,b], Yanan Chen[a], Zijian Liu[a], Jie Cai[c], Conglin Zhang[d], Yunxue Jin[e], Qingfeng Guan[a,*], Nan Zhao[a,*]

[a] School of Materials Science and Engineering, Jiangsu University, Zhenjiang 212013, China
[b] Department of Mechanical and Materials Engineering, Portland State University, Portland, OR 97207-0751, USA
[c] Engineering Institute of Advanced Manufacturing and Modern Equipment Technology, Jiangsu University, Zhenjiang 212013, China
[d] School of Materials Science and Engineering, Yancheng Institute of Technology, Yancheng 224051, China
[e] School of Materials Science and Engineering, Jiangsu University of Science and Tenology, Zhenjiang 212003, China

ARTICLE INFO

Keywords:
CrFeCoNiMo high entropy alloy
High current pulsed electron beam (HCPEB)
Microstructural modifications
Mechanical properties
Corrosion resistance

ABSTRACT

The surface of non-equiatomic CrFeCoNiMo high entropy alloy (HEA) was irradiated by high-current pulsed electron beam (HCPEB). Microstructure, mechanical properties and corrosion resistance of the CrFeCoNiMo HEA before and after HCPEB irradiation were studied systematically. The results of XRD analysis indicated that the surface of the irradiated samples exhibited preferential orientation on (1 1 1) and (2 0 0). Microstructure observations revealed that a compact remelted layer was formed on the surface of the alloy after HCPEB irradiation, the thickness of the remelted layer rose as the increase of pulse numbers. Besides, numerous nano σ particles, nanocrystallites with an average size about 109 nm and abundant deformed structures also appeared in the remelted layer. The mechanical properties of CrFeCoNiMo alloy were significantly enhanced after HCPEB treatment, which was mainly ascribed to intense plastic deformation via stress, sub-grain strengthening along with precipitation hardening. Electrochemical results demonstrated that all the irradiated specimens had a positive potential and a lower current density in 3.5 wt% NaCl solution compared with the untreated sample. The homogenized surface and the efficient eliminating of the local concentration of Cr element jointly contributed to the improvement of corrosion resistance.

1. Introduction

Lately, the intelligent and multi-functional of agricultural machinery has been rapidly developed, however, the key components are prone to wear and corrosion in severe working environments, which greatly shortens the lifetime of agricultural machinery [1]. As a result, the demand for materials with outstanding mechanical properties and corrosion resistance is continuously increasing, so that the facilities can be operated in harsh environments [2]. High entropy alloys (HEAs) have been a hot topic of extensive research on account of their unique microstructure and excellent properties [3]. By contrast with traditional alloys, HEAs are composed usually of five or more principal elements in a proximately equiatomic ratio (5–35 at.%). Existing multi-component phase diagrams indicate that a considerable number of involved components in HEAs may induce the formation of several brittle phases and complex intermetallic compounds [4]. Against expectation, simple solid solutions with face-centered cubic (FCC) or body-centered cubic (BCC) structure are stabilized preferentially on account of the high mixing entropy effect [5]. Due to this distinctive microstructure, HEAs typically have exceptional properties, such as brilliant thermal stability, high strength and hardness, outstanding wear resistance and excellent corrosion resistance [6].

Among various HEAs, CoCrFeNi and its ramifications was one of the first HEAs that was under extensive examination [7–13]. Liu et al. studied the effect of Al, Ti, Nb and Mo elements on the precipitation hardening behavior of ductile CoCrFeNi alloy, found that the molybdenum has the most effective strengthening effect on the CoCrFeNi matrix without reducing too much ductility [11]. Chou et al. reported that the addition of Mo improved the pitting resistance of $Co_{1.5}CrFeNi_{1.5}Ti_{0.5}Mo_x$ alloys in NaCl solution, and the $Mo_{0.1}$ alloy exhibited the best corrosion resistance [12]. Zhuang et al. investigated the effect of molybdenum content on microstructure and mechanical properties of Al0.5CoCrFeMoxNi high entropy alloy. It was found that the (Cr, Mo) enriched σ phase increased as the Mo content increased,

* Corresponding authors.
E-mail addresses: lvp@mail.ujs.edu.cn (P. Lyu), caijie@ujs.edu.cn (J. Cai), guanqf@ujs.edu.cn (Q. Guan), zhaonan@ujs.edu.cn (N. Zhao).

https://doi.org/10.1016/j.apsusc.2019.144453
Received 6 August 2019; Received in revised form 26 September 2019; Accepted 18 October 2019
Available online 28 October 2019
0169-4332/

Table 1
The parameters of HCPEB process.

Accelerated voltage (KeV)	Current pulse duration (μs)	Energy density ($J{\cdot}cm^{-2}$)	Beam diameter (mm)	Pulse interval (s)	Vacuum (Pa)
27	1.5	4	60	8	5×10^{-3}

which enhanced the hardness and compressive strength of the alloy, but caused a degradation of the ductility. The $Mo_{0.3}$ alloy had balanced properties of compressive strength and ductility [13].

The performances of alloy are decided by its microstructure, which is related to the synthesizing routes [4]. A variety of preparation methods have been adopted to fabricating HEAs [14], including vacuum arc melting and casting, laser cladding and powder metallurgy. Generally, HEAs are produced by vacuum arc melting and casting due to their easy availability and low cost. However, high entropy alloys prepared by this route is difficult to avoid the performance deficiencies such as shrinkage porosity, coarse dendritic microstructure and the chemical heterogeneity. The HEAs prepared by powder metallurgy process with excellent microstructural and compositional homogeneity compared with those of HEAs fabricated by the arc-melting and casting process [14]. Nevertheless, there are some micro-defects such as pores and unmelted particles, which limited the performances of the HEAs. To eliminate these defects, surface modification has been recognized as an effective method to drastically optimize the microstructure and significantly improve the overall performance of the surface. Some scholars applied laser remelting technology to treat plasma-sprayed high-entropy alloy coatings. The results found that the microstructure of the surface was completely modified, the elemental composition became fairly homogeneous, and the hardness and wear resistance were improved [15–17].

High-current pulsed electron beam (HCPEB) is a relatively new non-equilibrium technique, and its energy efficiency is much higher than that of the laser beams [18–24]. During the irradiation of HCPEB, high energy (10^8–10^9 W/cm^2) can be deposited in the surface layer within a very short time (less than tens microseconds), causing super-fast heating, melting, even evaporation, then followed by a rapid solidification and cooling [21]. The non-equilibrium temperature field combined with thermal stress effect, remarkably refine the surface microstructures of the modified layer; and the subsurface of the material undergoes intense and rapid deformation, a high density and diverse crystal defects can be formed on the surface [23]. Moreover, HCPEB treatment can package the surface, eliminate surface voids, and form a dense and uniform remelted protective layer [24]. Many scholars at home and abroad have applied high current pulsed electron beam technology to carry out the surface treatment of materials, and the comprehensive performance of the surface of the material has been improved [19–24]. Therefore, HCPEB irradiation is expected to avoid the inherent shortcomings of bulk metallurgy, further improve the comprehensive performance of high-entropy alloys, and increase its potential industrial application as structural materials.

Hence, in this work, HCPEB irradiation was acted on the CrFeCoNiMo HEA which was prepared by powder metallurgy. A detailed characterization of the microstructural evolution of CrFeCoNiMo alloy before and after HCPEB irradiation was investigated. The strengthening mechanisms of mechanical properties and corrosion resistance were also examined in detail. In some respects, this work provides a necessary theoretical and experimental reference for subsequent scientific research and practical application of the CrFeCoNiMo alloy.

2. Experimental details

The powder with a nominal composition $Cr_{23.81}Fe_{23.81}Co_{23.81}Ni_{23.81}Mo_{4.76}$ (all compositions are in atomic percent (at.%)) was produced by ball milling of Cr, Fe, Co, Ni and Mo pure metal powders. Each elemental powder had a purity of exceeding 99.99% and a particle size of less than 200 mesh. The raw powders were milled for 6 h in a high-energy planetary ball milling device (YXQM-4L) under a high purity argon gas atmosphere. The ball to powder ratio was 10:1 and the ball milling speed was 300 rpm. The milled powders were then consolidated by spark plasma sintering (SPS) system (FCT HP D5, Germany) under vacuum (< 8 Pa). While the powders were heated at a heating rate of 100 °C min^{-1} and the pressure was applied to 30 MPa, followed by 20 min of holding time at 1000 °C and 30 MPa.

The initial CrFeCoNiMo alloy was cut into Φ8 × 5 mm columns and annealed to 900 °C for 5 h. Mechanical grinding and polishing were then practiced on one cutting surface of the specimens. Afterward, a "HOPE-I" type HCPEB equipment was adopted to irradiate the CrFeCoNiMo samples with 15 and 30 pulses, respectively. The parameters of HCPEB irradiation are given in Table 1.

The phase compositions of the samples were identified by X-ray diffraction (XRD, Rigaku D/max-2500/pc, 45 kV, 40 mA) with Cu Kα radiation (λ = 0.154 nm). Scanning electron microscopy (SEM) (FEI nano 450) equipped with energy dispersive X-ray spectrometer (EDS) was adopted to characterize the microstructure and chemical constitutions of the sintered and irradiated samples. The more details about microstructures in the modified layers were investigated using a JEM-2100 transmission electron microscope (TEM). The disc samples for TEM observation were prepared by one-side mechanical thinning to about 30–50 μm and subsequent ion beam thinning from the untreated side.

Microhardness test was determined by a Vickers hardness device (FAST 500) under 0.98 N loading for 15 s; six measurements were averaged to ensure accuracy. The wear test was operated at room temperature on a ball-on-disc equipment (SFT-2 M) with a GCr15 ball (Φ4 mm), which was worn as friction pair to on the CrFeCoNiMo specimens at 300 rpm for 10 min under a constant load of 5 N. The wear rate of samples was calculated, and the morphology of worn surface was investigated using SEM.

Corrosion study was examined by a CHI760C electrochemical workstation in 3.5 wt% NaCl solution at room temperature. A conventional three-electrode cell was used, specimen as a working electrode, a saturated calomel electrode (SCE) as the standard electrode and a platinum net as an auxiliary electrode. Before the standard potentiodynamic polarization measurement, samples were placed in the electrolyte solution for 30 min at open circuit potential to stabilize the corrosion potential.

3. Results and discussions

3.1. Phase identification

The XRD analysis of the CrFeCoNiMo HEA before and after HCPEB irradiation is shown in Fig. 1. From Fig. 1(a), it is evident that all alloys were principally consisted of fcc solid solution which can be ascribed to the high entropy effect. Furthermore, some weak peaks between the fcc (1 1 1) and (2 0 0) peaks were detected, these diffraction peaks were identified as σ secondary phase (a = 9.17 Å, c = 4.741 Å, c/a = 0.517), and its structure is close to a tetragonal FeCrMo phase [10]. After the HCPEB bombardment, the diffraction peaks were observed to change obviously. The intensity of (1 1 1) diffraction peak declined after irradiation while that of (2 0 0) peak gradually increased, which indicates that the surface of irradiated samples exhibited preferential orientation.

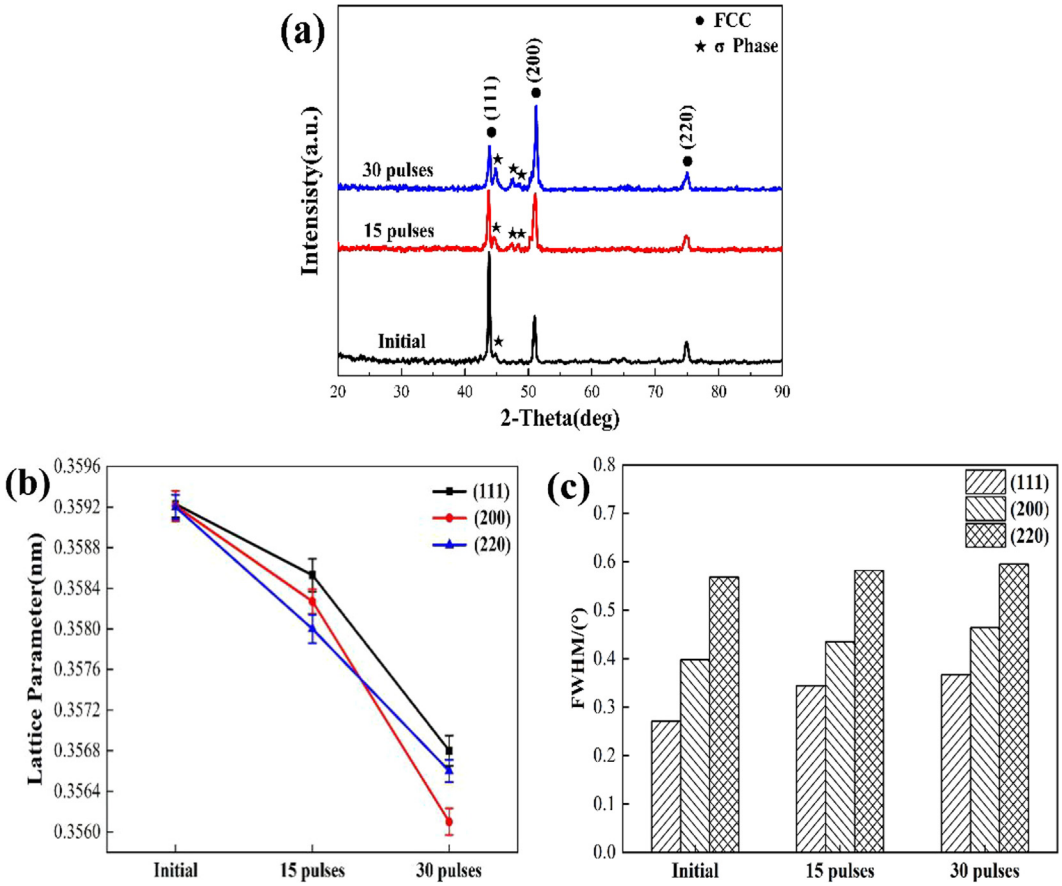

Fig. 1. The XRD analysis of the CrFeCoNiMo samples before and after HCPEB irradiation. XRD patterns; (b) fcc lattice parameters; (c) the variation in the maximum value of the half-width with different pulses.

The texture coefficient can be used to determine the orientation change of the surface structures after HCPEB irradiation [25].

$$T = \frac{I_{hkl}/I^0_{hkl}}{(1/n)\sum_{h'k'l'}(I_{h'k'l'}/I^0_{h'k'l'})} \quad (1)$$

where I_{hkl} and I^0_{hkl} are the diffraction intensities of the (*hkl*) crystal planes of the irradiated sample and the untreated sample, and n is the total number of crystal planes. When the T_{hkl} of an individual reflection is larger than 1, it indicates that the crystal plane has a preferred orientation after irradiation treatment. The texture coefficient of (1 1 1), (2 0 0) and (2 2 0) crystal planes are calculated and shown in Table 2. As can be seen, the irradiated samples had a preferred orientation on the (1 1 1) and (2 0 0) crystal planes after HCPEB treatment. Extremely high energy is shifted into the surface of the material instantaneously, which leads to a quite rapid melting (even evaporating) and follows by a rapid solidification. In crystallography, it is believed that this rapid non-equilibrium treatment may change the growth orientation of the grains and thus change its texture properties.

From a closer observation, the irradiated peaks had a minor shift to a high angle. According to Bragg's law, the lattice parameters were computed and graphed in Fig. 1(b). The lattice parameters of HCPEB irradiated samples are lower than those of the initial sample. It is believed that some Mo and Cr atoms precipitated out from the supersaturated fcc solid solution and formed the σ phase during the non-equilibrium HCPEB irradiation process. Three samples were selected for each parameter to calculate the lattice parameters, and three measurements were averaged to ensure accuracy. Fig. 1(c) shows the variation in the maximum value of the half-width with the number of irradiation pulses. It is seen that Bragg diffraction peaks of irradiated samples were broadened compared to the untreated sample, which was consistent with the result of other studies [23,24]. HCPEB irradiation induced rapid melting and solidifying on the surface layer, which resulted in the grains of the irradiated surface to be remarkably refined, and further lead to broadening of peaks.

Table 2
Texture coefficients of crystal planes after HCPEB irradiation.

Pulse number	(1 1 1)	(2 0 0)	(2 2 0)
15	1.639	1.217	0.418
30	1.282	1.783	0.497

3.2. Microstructure characterization

Fig. 2 gives the microstructure of the sintered CrFeCoNiMo HEA. From the secondary electron (SE) mode (Fig. 2(a)), the surface of the sintered sample was relatively dense and smooth. However, some coarse and continuous pore networks which were formed by interconnecting large-sized shrinkage cavities and many small-sized pores also appeared on the surface. It is well known that the necessary condition for metallurgical sintering was that mass transfer must occur between particles [1]. The sintering process was carried out at a relatively low heating temperature resulting in a lack of the diffusion driving force of atoms in alloy, the atomic diffusion was slow, so that a large number of pores existed in the powder particles. These pores were interconnected with cavities to form pore networks.

Besides, in the backscattered electron (BSE) image (Fig. 2(b)), some white and black regions were observed in the fcc matrix. Table 3 lists the elemental compositions of the structures labeled as A, B, and C in

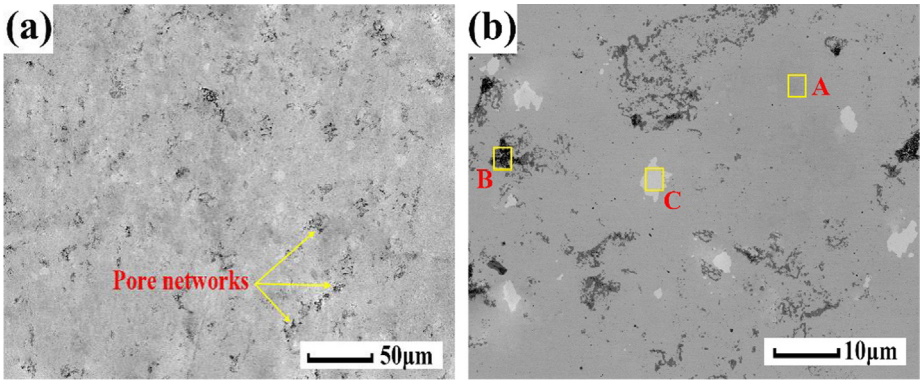

Fig. 2. The morphology of the sintered CrFeCoNiMo HEA: (a) secondary electron image; (b) backscattered electron image.

Table 3
The elemental compositions of the structures labeled as A, B and C in Fig. 2. (At. %).

Region	Cr	Fe	Co	Ni	Mo	O
Nominal	23.81	23.81	23.81	23.81	4.76	–
A	13.07	28.81	27.34	29.40	1.38	–
B	39.39	16.66	13.50	9.35	2.91	18.19
C	23.52	17.80	18.69	13.24	26.75	–

Fig. 2(b). The composition of the fcc matrix (region A) deviated from the nominal composition, combined with XRD analysis, and it could be deemed that the microstructure composed of other phases or precipitations. In area B, some partially reacted powders inserted in the pore networks, the powders contained mainly Cr element via EDS. Meanwhile, the oxygen element was also detected in region B, indicating that part of the powders may be oxidized during high energy ball milling. Besides, few (Cr, Mo)-rich particles (area C) were discovered in the matrix, which was detected as the σ phase via XRD, as shown in Fig. 1(a). Connected pore networks and unmelted powders will limit the overall performances of CrFeCoNiMo HEA, particularly under the destructive corrosion condition.

Fig. 3 displays the surface morphology of CrFeCoNiMo irradiated samples. The 15-pulsed sample, as shown in Fig. 3(a), numerous craters formed on the surface of irradiated samples, it turned out that the complete melting of the surface after HCPEB irradiation. Previous studies demonstrated that crater was a characteristic feature on many HCPEB-irradiated surfaces of metal materials, and its formation mechanism could be summarized as the non-homogeneous local sublayer melting and subsequent eruption through the outer surface [26,27]. During the HCPEB treatment, the subsurface of the material preferentially melted and formed small molten droplets, which caused the volume of the material in this region to expand rapidly. The expansion driving force on the molten metal droplets was larger than the surface resistance, and the molten droplets burst through the surface and rapidly solidified to form a crater during the subsequent extremely rapid cooling process. Meanwhile, it had been well established that the crater was more susceptible to nucleate at the microstructure irregularities, such as various structural defects and second phase particles [19,28]. With the number of pulses increased to 30 (Fig. 3(b), some craters which formed at the beginning of the irradiation had been further fused or removed by the multiple HCPEB pulses owing to the accumulation of more energy. Three samples were selected for each parameter, and five different regions of each sample were taken at the same magnification. The measurement is the average value of the results for 15 different regions (the area of image is 2.87×10^{-4} cm^2, the length is 205 μm and the width is 140 μm). Fig. 3(c) presents the density and average size of craters of 15-pulsed and 30 pulsed samples, the size and numbers of craters on the 30-pulsed surface were decreased, suggesting that the surface of the 30-pulsed sample became smoother and denser.

Fig. 3(d) is a backscattered electron (BSE) image of 30 irradiated samples, it can be seen that the microstructure exhibited a uniform contrast on the surface of the 30-pulsed sample. Fig. 3(e) provides the element mapping analysis of the area in Fig. 3(d). It revealed that all the elements were uniformly distributed on the irradiated surface. This suggested that the unmelted Cr powder on the surface of sintered CrFeCoNiMo alloy was dissolved and the local concentration of Cr element was eliminated effectively during HCPEB irradiation process. The element compositions of CrFeCoNiMo HEA after HCPEB treatment by different pulses are listed in Table. 4. The result showed that a good homogeneity of the chemical composition in the irradiated samples. Compared with the 15-pulsed sample, the generated composition of the 30-pulsed specimen was closer to the nominal composition. Therefore, the results show that HCPEB treatment facilitated the composition of treated surfaces to become more homogeneous.

The cross-sectional SEM images of the irradiated specimens are illustrated in Fig. 4. The surface can be categorized into distinct two-layer: the remelted layer and the matrix. Thereinto, the most apparent difference between the two layers was that a large number of ultrafine particles embed in the modified layer. As the number of HCPEB pulses increased from 15 to 30, the thickness of the remelted layer was thickened from about 2.9 μm to 5.4 μm. The gradual increase in the thickness of the remelted layer was the result of heat accumulation in the subsurface and the deepening of the inward diffusion when multiple HCPEB pulses are performed at a short interval [29].

The TEM technique was adopted to further investigated the fine microstructure in the remelted layer in detail. Fig. 5 presents the TEM micrographs corresponding to the remelted layer of the 30-pulsed sample. The ultrafine grains having an average size of 110 nm were formed in the top surface layer after 30 pulses (Fig. 5(a)). The main reason ~~is~~ was that a large number of nucleations were formed on the remelting surface layer, but the cooling rate was too fast so that these crystal nuclei had not enough time to grow up, resulting in the formation of ultrafine grains or nanocrystalline structure on the surface [30]. Meanwhile, plenty of step structures were observed inside the grains, and the corresponding selected area electron diffraction (SAED) pattern are shown in Fig. 5(b). It is found that the diffraction spots were symmetrically distributed along the {1 1 1} plane, forming a typical twin orientation relationship. The step structure ~~is~~ was a characteristic feature of deformation twins. The above experimental results demonstrates that the step structures induced by HCPEB irradiation ~~are~~ were deformation twins. As seen in Fig. 5 (c), there were plenty of circular particles in the 30-pulsed sample, their sizes were in the range of 5–105 nm and the mean size was 43 nm. These particles were identified as σ phase according to the selected area diffraction (SAED) pattern (Fig. 5(d)), which was consistent with the XRD result in Fig. 1(a). It is worth noting that although these particles preferentially nucleate in the grain boundaries or inside equiaxed-grains, they are in discrete and

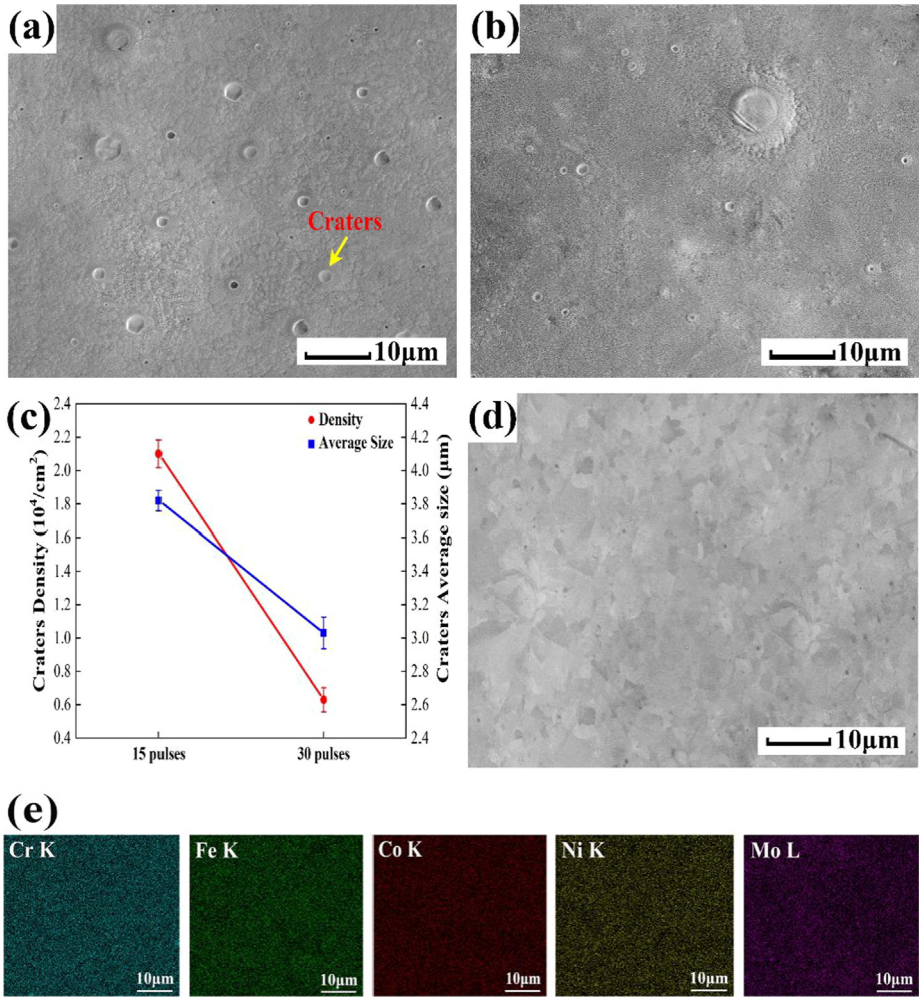

Fig. 3. The SEM images and EDS analysis of HCPEB CrFeCoNiMo irradiated samples. (a) Surface SE image of 15 pulses, (b) surface SE image of 30 pulses, (c) the density and average size of craters, (d) surface BSE image of 30-pulsed sample, (e) the element mapping analysis of 30-pulsed sample.

Table 4
The element compositions of CrFeCoNiMo HEA treated by different pulses (At. %).

Samples	Cr	Fe	Co	Ni	Mo
Nominal	23.81	23.81	23.81	23.81	4.76
15 pulses	25.82	23.37	22.89	22.76	5.16
30 pulses	23.91	24.31	22.99	23.91	4.88

individual, which contributes to excellent mechanical properties [31].

Fig. 6 shows TEM bright-field images corresponding to the remelted layer of the 30-pulsed sample. Except the above-mentioned deformed twins, a variety of deformation structures such as subgrains and dislocations were also observed, which was due to a high-intensity thermal stress induced by HCPEB irradiation resulting in intense plastic deformation of the material surface. From Fig. 6(a), some subgrains (marked by the yellow arrow) with a size of about 100 nm were seen in the remelted layer. Fig. 6(c) and (d) shows the various dislocations of the irradiated sample after 30-pulsed irradiation. After HCPEB

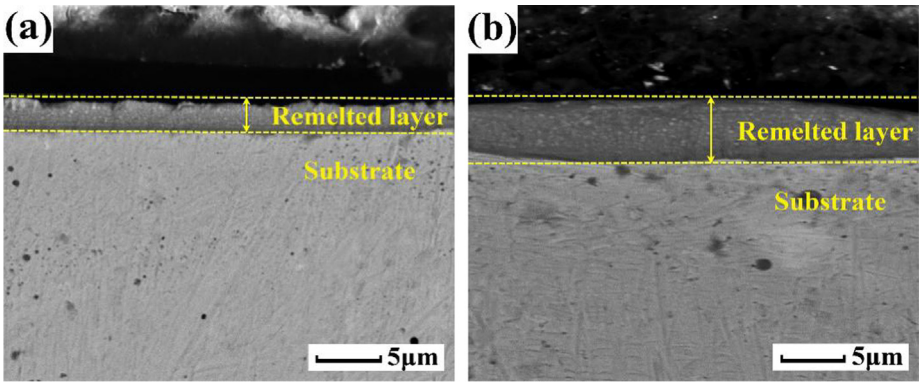

Fig. 4. Cross-sectional SEM images of the HCPEB irradiated CrFeCoNiMo samples with 15 pulses (a) and 30 pulses (b).

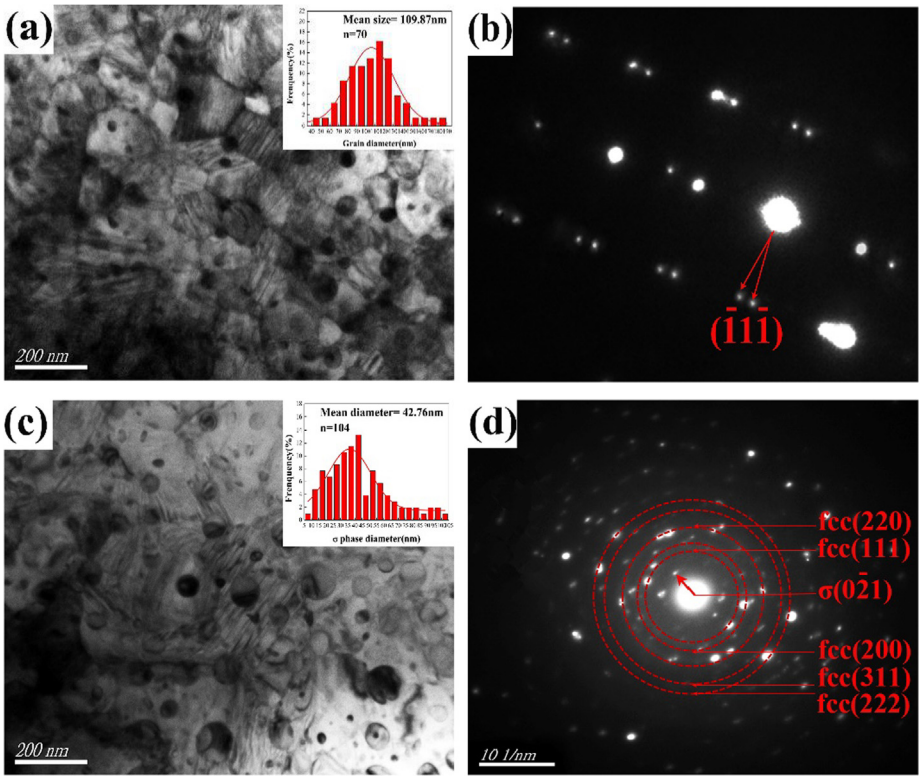

Fig. 5. TEM micrographs corresponding to the remelted layer of the 30-pulsed sample. (a) Ultrafine grains, (b) SAED pattern of step structures, (c) circular particles and its corresponding SAED pattern (d).

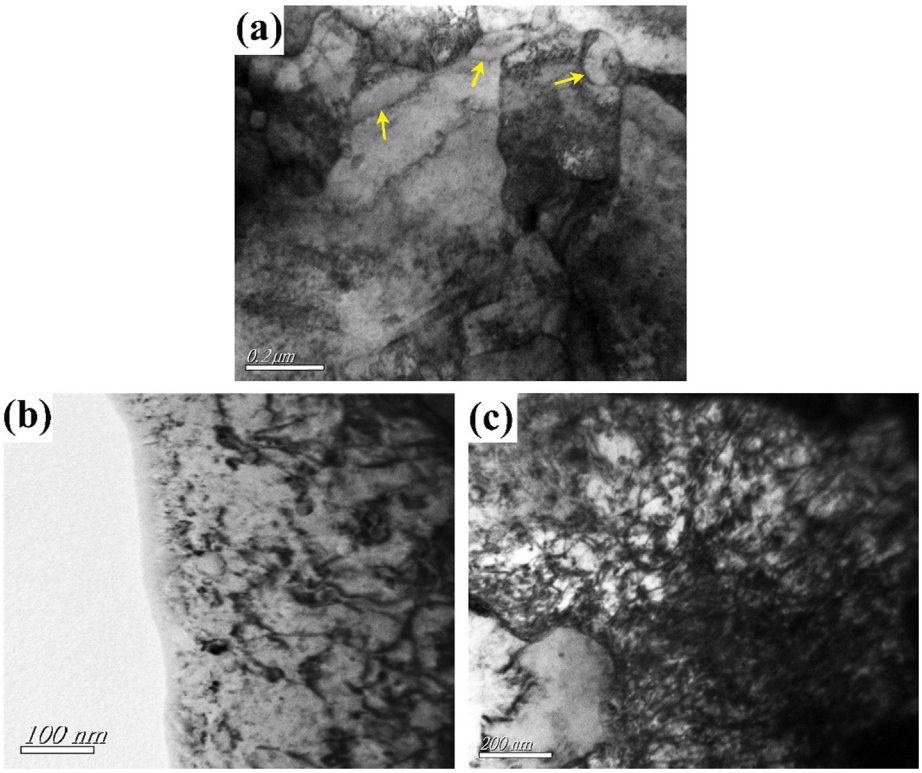

Fig. 6. TEM bright-field images corresponding to the remelted layer of 30-pulsed sample. (a) subgrains, (b and c) dislocations.

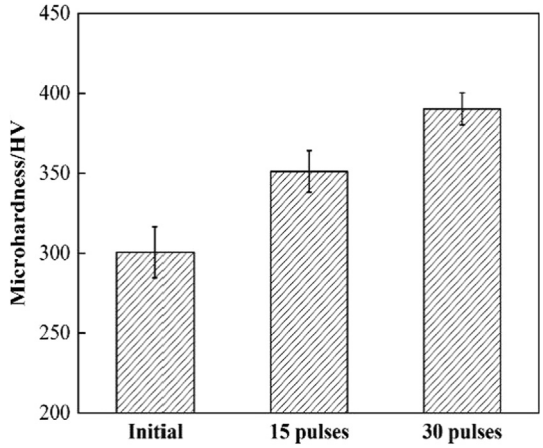

Fig. 7. Microhardness measurements of CrFeCoNiMo samples before and after HCPEB irradiation.

irradiation, few dislocations formed in the local area, while the density of dislocations in some regions was extremely high, and entangled dislocations almost filled the entire grain.

3.3. Mechanical properties

Fig. 7 shows the variations in the microhardness of the CrFeCoNiMo alloy before and after HCPEB irradiation, and the hardness was on the rise after HCPEB treatment. The hardness value of the initial sample was rather low, around 300.5 HV, after 15-pulsed irradiation, the hardness of the sample was increased apparently, about 351.1 HV. As the number of pulses multiplied by 30, the hardness value further increased, the maximum value was 392.3HV, which was 30.5% greater than that of the untreated one. Therefore, the hardness of CrFeCoNiMo HEA was noticeably enhanced by HCPEB irradiation.

The material hardening can be interpreted through three factors as follows. Firstly, as above mentioned, many ultra-grains even nanocrystalline (Fig. 5(a)) were formed on the remelted layer after HCPEB irradiation. The refined grains were resulting in the improvement of the hardness due to the effect of subgrain strengthening [32]. Secondly, the uniform dispersion of the nano hard σ particles played a dominant role in the strengthening of CrFeCoNiMo alloy, which was known as precipitation hardening. These hard σ phases not only acted as a barrier to the dislocation motion but also reduced the capillary driving force for grain growth [24]. Combined with the XRD results, the volume fraction of the σ phase rose as the number of pulses increased, which is the main reason why the hardness of 30-pulsed sample ~~is~~ was higher than that of the 15-pulsed sample. Thirdly, the high-intensity thermal stress induced by HCPEB irradiation yielded extremely strong and rapid plastic deformation (Fig. 6). The presence of deformation structures hindered the movement of dislocations and enhanced the hardness by stress strengthening [32].

The wear behavior of the initial and HCPEB irradiated samples are shown in Fig. 8. Fig. 8(a) plots the variation of the friction coefficient (COF) with wearing time for specimens before and after HCPEB irradiation. The friction coefficient of sintered CrFeCoNiMo alloy was found as 0.61; the value of COF was dramatically declined to 0.16 after 30-pulsed irradiation. The superior wear resistance of treated specimens concerning the initial sample could be demonstrated from the wear rate shown in Fig. 8(b). The wear rate of the untreated sample was 1.86×10^{-4} $mm^3 \cdot N^{-1} \cdot m^{-1}$, which was around 4–6 times higher than that of irradiated samples ($0.32–0.44 \times 10^{-4}$ $mm^3 \cdot N^{-1} \cdot m^{-1}$). Similar to the coefficient of friction, the wear rate was also decreased sharply as the pulse numbers increased. The reduction in the friction coefficient of the irradiated samples was mainly related to the enhanced hardness of the alloy. The wear resistance of materials is usually proportional to their hardness, which was in good agreement with the conclusion of Khruschov [33].

Fig. 9 presents the worn traces of the friction surface of the CrFeCoNiMo samples before and after irradiation. As seen in Fig. 9(a), the initial sample had a wear scratch of about 298 μm in width and 6 μm in depth, the wear scratch was deep and wide. For the irradiated samples, the width of the wear traces was less than 200 μm and the depth was 3 μm, which was only half of that of the untreated sample. Compared with the untreated sample, wear traces were shallower and narrower, indicating that the tribological property of the CrFeCoNiMo samples was significantly improved after HCPEB irradiation.

The degree of friction is related to the change in hardness and the resistance of the contact area [15]. The hardness of the initial sample was low, the matrix was firstly deformed and extruded, a large amount of debris gradually exposed on the surface, which resulted in the surface became rugged. Many isolated sharps and micro-convex areas existed on the surface due to the roughness of the surface increased. These sharps and small protrusions generated high stress and plastic flow on the contact point when the surface was in contact with the grinding ball, causing adhesion of the contact point. Meanwhile, those wear debris were more vulnerable to be oxidized owing to the generation friction heat during the sliding process. The temperature and the resistance of the contact area rose as the degree of adhesion increased, and more oxygen was adsorbed to the surface. This was the main reason why the surface to be severely oxidized. As above mentioned, the hardness of the σ phase ~~is~~ was higher than that of the FCC matrix. In the early stage of the sliding process, the matrix deformed and a large number of fine σ phases were gradually extruded, and these particles were not worn easily, thereby the friction coefficient was lower and

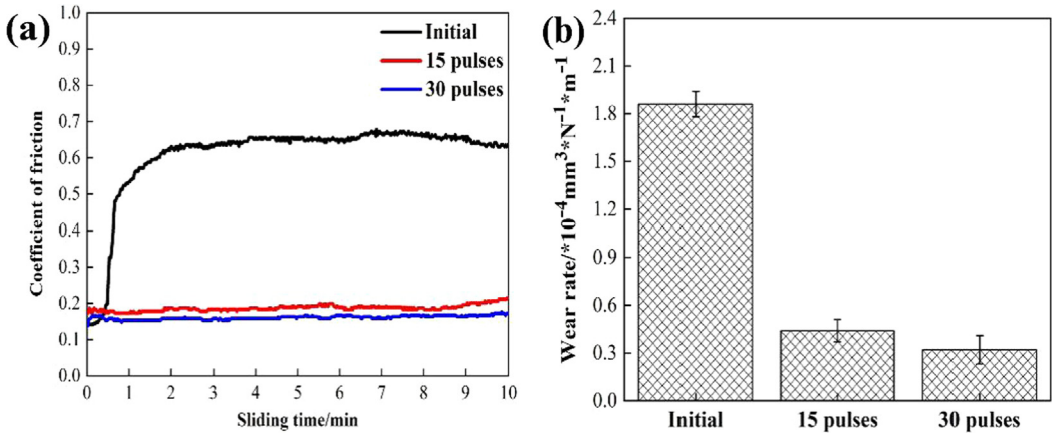

Fig. 8. Tribological behavior of the initial and HCPEB irradiated samples: (a) coefficient of friction, (b) wear rate.

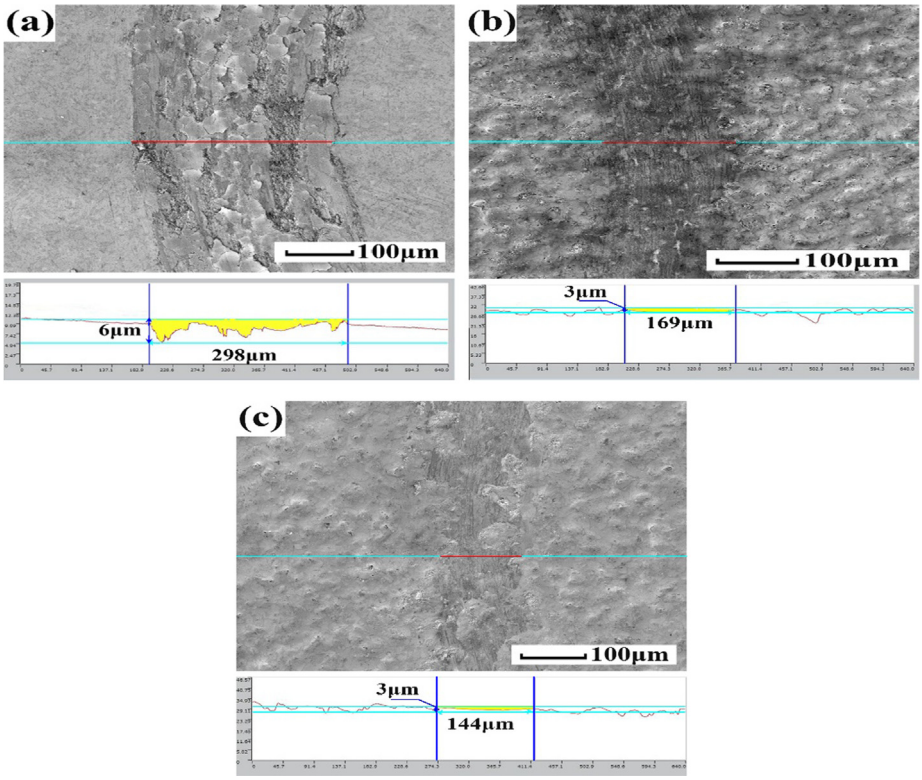

Fig. 9. The scratch profile of the surface of samples before and after HCPEB irradiation. (a) Initial, (b) 15 pulses, (c) 30 pulses.

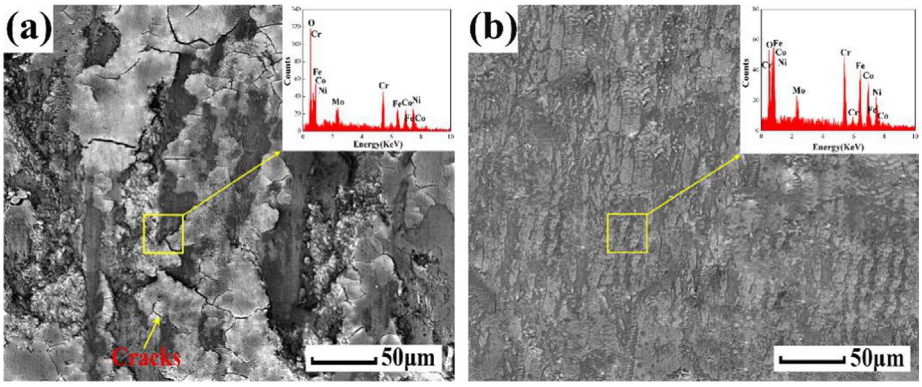

Fig. 10. The worn surface morphologies of sintered CrFeCoNiMo alloy and 30-pulsed irradiated samples.

remained stable. During the sliding process, these tiny particles were ground into fine wear debris and dispersed on the worn surface to form a mechanical friction layer with better lubrication, which inhibited the occurrence of severe wear, so that the abrasion of the surface could be reduced. Consequently, the improvement in wear resistance of CrFeCoNiMo HEA mainly owing to the enhanced hardness, and the formation of a thin oxide film along with the dispersion of hard σ phase also contributed to an improvement in wear resistance.

After the abrasion test, the worn surface profiles of sintered CrFeCoNiMo alloy and 30-pulsed irradiated sample were shown in Fig. 10, and in which the chemical components of the worn debris were also given. In Fig. 10(a), adhesive wear can be evidenced by cracks with the formation of patches of adhered material and delamination [34]. And lots of peeling fragments and abrasive debris/particles also found on the surface. Combining with EDS analysis of the worn surface, the worn surface of untreated alloy had a high oxygen content, which indicated that the worn surface ~~is~~ was oxidized due to the generation of frictional heat during the friction process. Hence, the wear mechanisms of sintered CrFeCoNiMo alloy could be deemed as adhesive wear accompanied by oxidative wear.

As seen in Fig. 10(b), the furrows on the worn surface of the irradiated sample were shallower than that of the untreated CrFeCoNiMo alloy, indicating that the irradiated samples possessed better tribological property. Meanwhile, some debris also appeared on the worn surface of the irradiated samples (Fig. 9(b) and (c)). These findings indicated that the irradiated samples were primarily subject to abrasive wear during the process of friction. The EDS analysis revealed that low oxygen element was resided in the worn surface, indicating the frictional surface was oxidized slightly during the wear process. It is believed that a thin oxide film was formed on the surface to avoid the direct contact of the grinding ball and alloy during abrasion.

3.4. Corrosion resistance

The polarization curves of the initial and HCPEB-irradiated CrFeCoNiMo samples in 3.5 wt% NaCl solution are given in Fig. 11, and the corresponding corrosion parameters are listed in Table 5. Compared with the initial sample, the polarization curves of both the 15-pulsed

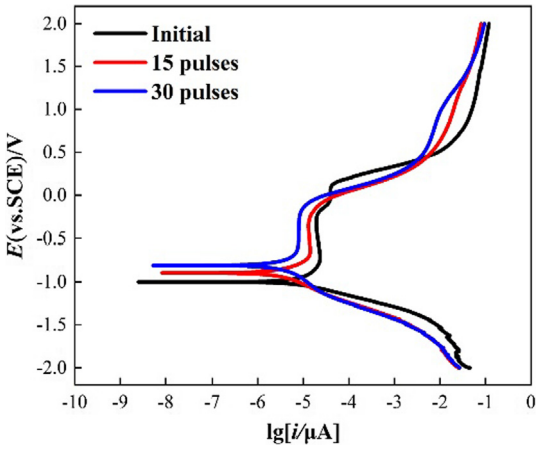

Fig. 11. The potentiodynamic polarization curves of the sintered and HCPEB-irradiated CrFeCoNiMo samples in 3.5 wt% NaCl solution.

Table 5
The electrochemical measurements of the initial and irradiated samples.

Samples	I_{corr}/μA·cm^{-2}	E_{corr}/V
Initial	15.388	−1.000
15 pulses	6.862	−0.895
30 pulses	6.059	−0.807

and 30-pulsed samples shifted to the direction of more positive potential and lower current density. The I_{corr} reflects the corrosion dynamics that is proportional to the corrosion rate [35], as can be seen from Table 4, the I_{corr} of the irradiated samples was an order of magnitude lower than that of the initial sample (15.388 μA·cm^{-2}), indicating that the corrosion rate of HCPEB-irradiated samples was decreased. Furthermore, the E_{corr} of treated samples rose as the increase of the pulses, and the higher values of the E_{corr} indicates the samples ~~are~~ were not susceptible to be corroded [35]. Therefore, the experimental results clarified that the irradiated samples possessed better corrosion resistance compared to untreated CrFeCoNiMo alloy.

For the initial CrFeCoNiMo alloy, the formation of the oxide film via the dissolution of individual elements on the surface. However, the rough and continuous pore networks and unmelted Cr powder on the surface made the oxide film to be discontinuous and loose. This porous structure also supplied a convenient pathway for the intrusion of corrosive anions (Cl^-) so that Cl^- can more easily diffuse into the interior of the sample, even reaching the matrix, which resulted in the dissolution of the passive film. Subsequently, the passive film was reformed and redissolved in the chloride ion environment, which yielding the passive film was continuously dissolved and eventually to be corroded. Besides, localized component segregation was caused by the existence of unmelted Cr powder, which offered more potential for galvanic coupling, which accelerated the corrosion of the material.

According to the literature [30,36,37], the enhancement corrosion resistance irradiated samples was principally ascribed to the efficient cleaning of the irradiated surface from undesirable inclusions, deduction or disappearance of craters and formation of a homogeneous and stable protective layer. In this work, the mechanism of improved corrosion resistance of HCPEB irradiated CrFeCoNiMo samples were similar to the results of the above literature. During HCPEB irradiation process, the unmelted Cr powder in the surface layer was dissolved, and the local concentration of Cr element was eliminated effectively. Thus the sensitive points of corrosion were gradually cleared, which can decrease the potential of corrosion pitting [28,30]. After that, the remelting surface layer has undergone ultra-fast cooling and solidification when treated with multiple HCPEB pulses of a short interval. Thus, a relatively homogeneous composition distribution can be retained along with the formation of the remelted layer [38]. Other authors have suggested that the formation of a homogeneous layer at the top surface gave less potential for galvanic coupling [39]. Therefore, an improved corrosion resistance of irradiated samples was attributed to the combined effects of the effifficient eliminating of the local concentration of Cr on the surface along with the homogenized surface. After HCPEB irradiation, CrFeCoNiMo high entropy alloy had high hardness, excellent wear resistance and corrosion resistance. It could meet the performance demand of key components of agricultural machinery and be applied to high-end agricultural machinery, such as the blades for rotary tillers.

3.5. Modification mechanism

During the HCPEB irradiation process, the extremely high-energy particle flow instantaneously acted on the surface of the CrFeCoNiMo HEA by the accelerating electron beam as an energy carrier to form a heat-affected zone with a very high temperature gradient. At the same time, at a sufficiently high heating temperature, a series of physical and chemical processes were generated in the heated surface layer such as quite rapid melting, evaporating and melt eruption [20]. After HCPEB irradiation, the surface undergone extremely rapid cooling and solidification process. Also, the subsurface of the CrFeCoNiMo HEA undergone intense and rapid deformation, forming high density of craters, ultra-fine grains, deformed twins and dislocation. Due to the microstrucure modified by HCPEB irradiation, the CrFeCoNiMo HEA had high hardness and excellent wear resistance. Moreover, As the number of irradiation pulses increases, a relatively homogeneous composition distribution can be retained along with the formation of the remelted layer. It means that, the surface of CrFeCoNiMo HEA was packaged after HCPEB treatment. Therefore, the corrosion resistance was improved.

4. Conclusion

The relationship between microstructure and properties of the HCPEB irradiated CrFeCoNiMo alloy with different pulses was systematically investigated. The main results can be generalized as follows:

(1) The surface of the sintered alloy was relatively smooth, and some defects such as unmelted powder and pore networks were observed. After HCPEB irradiation, a 3–5 μm thick nanocrystalline remelting layer was formed on the irradiated samples, inside which the grains and σ phase were refined. Moreover, abundant structure defects such as dislocations and subgrains were also detected.
(2) The HCPEB irradiated samples exhibited higher microhardness values and better wear properties, and the performances were improved as the pulse numbers increased. The improvement of surface hardness was mainly ascribed to subgrain strengthening, dislocation strengthening and precipitation hardening. The reduction in the friction coefficient of the irradiated samples is primarily related to the enhanced hardness of the alloy.
(3) For the irradiated specimens, the E_{corr} showed a rising trend, while the I_{corr} was decreased by nearly an order of magnitude, which disclosed that the corrosion resistance of the irradiated samples was improved evidently. The homogenized surface as well as the efficient eliminating of the local concentration of Cr element jointly contributed to the enhancement of corrosion resistance.

Declaration of Competing Interest

The authors declared that there is no conflict of interest.

Acknowledgments

This work was supported by National Natural Science Foundation of

China (No. 51601071), the Postdoctoral Foundation of Jiangsu Province (No. 2018K025B), the Youth Talent Development Program of Jiangsu University, Postgraduate Innovation Programs Foundation of Jiangsu Province (No. KYCX18-2236), Key University Science Research Project of Jiangsu Province (16KJB430009) and Senior Talent Foundation of Jiangsu University (15JDG078).

References

[1] Y. Zhang, T.T. Zuo, Z. Tang, M.C. Gao, K.A. Dahmen, P.K. Liaw, Z.P. Lu, Microstructures and properties of high-entropy alloys, Prog. Mater. Sci. 61 (2014) 1–93, https://doi.org/10.1016/j.pmatsci.2013.10.001.

[2] K. Kuwabara, H. Shiratori, T. Fujieda, K. Yamamaka, Y. Koizumi, A. Chiba, Mechanical and corrosion properties of AlCoCrFeNi high-entropy alloy fabricated with selective electron beam melting, Additive Manuf. 23 (2018) 264–271, https://doi.org/10.1016/j.addma.2018.06.006.

[3] N. Eissmann, B. Kloden, T. Weissgarber, B. Kieback, High-entropy alloy CoCrFeMnNi produced by powder metallurgy, Powder Metall. 60 (2017) 1–14, https://doi.org/10.1080/00325899.2017.1318480.

[4] J.B. Li, B. Gao, S. Tang, B. Liu, Y. Liu, Y.T. Wang, J.W. Wang, High temperature deformation behavior of carbon containing FeCoCrNiMn high entropy alloy, J. Alloys Compd. 747 (2018) 571–579, https://doi.org/10.1016/j.jallcom.2018.02.332.

[5] H.Y. Diao, R. Feng, K.A. Dahmen, P.K. Liaw, Fundamental deformation behavior in high-entropy alloys: an overview, Curr. Opin. Solid. St. M. 21 (2017) 252–266, https://doi.org/10.1016/j.cossms.2017.08.003.

[6] M.H. Tsai, J.W. Yeh, High-Entropy Alloys: A Critical Review, Mater. Res. Lett. 2 (2014) 107–123, https://doi.org/10.1080/21663831.2014.912690.

[7] P. Sathiyamoorthi, J. Basu, S. Kashyap, K.G. Pradeep, R.S. Kottada, Thermal stability and grain boundary strengthening in ultrafine-grained CoCrFeNi high entropy alloy composite, Mater. Des. 134 (2017) 426–433, https://doi.org/10.1016/j.matdes.2017.08.053.

[8] J.W. Wang, Y. Liu, B. Liu, Y. Wang, Y.K. Cao, T.C. Li, R. Zhou, Flow behavior and microstructures of powder metallurgical CrFeCoNiMo0.2 high entropy alloy during high temperature deformation, Mater. Sci. Eng. A. 689 (2017) 233–242, https://doi.org/10.1016/j.msea.2017.02.064.

[9] M.Y. Zhang, W. Zhang, Y. Liu, B. Liu, J.S. Wang, FeCoCrNiMo high-entropy alloys prepared by powder metallurgy processing for diamond tool applications, Powder Metall. 61 (2018) 123–130, https://doi.org/10.1080/00325899.2018.1429044.

[10] T.T. Shun, L.Y. Chang, M.H. Shiu, Microstructure and mechanical properties of multiprincipal component CoCrFeNiMox alloys, Mater. Charact. 70 (2012) 63–67, https://doi.org/10.1016/j.matchar.2012.05.005.

[11] W.H. Liu, T. Yang, C.T. Liu, Precipitation hardening in CoCrFeNi-based high entropy alloys, Mater. Chem. Phys. 210 (2017) 2–11, https://doi.org/10.1016/j.matchemphys.2017.07.037.

[12] Y.L. Chou, J.W. Yeh, H.C. Shih, The effect of molybdenum on the corrosion behaviour of the high-entropy alloys Co1.5CrFeNi1.5Ti0.5Mox in aqueous environments, Corros. Sci. 52 (8) (2010) 2571–2581, https://doi.org/10.1016/j.corsci.2010.04.004.

[13] Y.X. Zhuang, X.L. Zhang, X.Y. Gu, Effect of molybdenum on phases, microstructure and mechanical properties of Al0.5CoCrFeMoxNi high entropy alloys, J. Alloys Compd. 743 (2018) 514–522, https://doi.org/10.1016/j.jallcom.2018.02.003.

[14] K. Byungchul, L. Junho, J.R. Ho, H.H. Soon, Ultra-high strength WNbMoTaV high-entropy alloys with fine grain structure fabricated by powder metallurgical process, Mater. Sci. Eng A. 712 (2018) 616–624, https://doi.org/10.1016/j.msea.2017.12.021.

[15] B.Q. Jin, N.N. Zhang, S. Guan, Y. Zhang, D.Y. Li, Microstructure and properties of laser remelting FeCoCrNiAl0.5Six high-entropy alloy coatings, Surf. Coat. Tech. 349 (2018) 867–873, https://doi.org/10.1016/j.surfcoat.2018.06.032.

[16] D.Y. Lin, N.N. Zhang, B. He, B.Q. Jin, Yue Zhang, D.Y. Li, F.Y. Dong, Influence of laser re-melting and vacuum heat treatment on plasma-sprayed FeCoCrNiAl alloy coatings, J. Iron Steel Res Int. 24 (2017) 1199–1205, https://doi.org/10.1016/S1006-706X(18)30018-9.

[17] C.M. Wang, J.X. Yu, Y. Zhang, Y. Yu, Phase evolution and solidification cracking sensibility in laser remelting treatment of the plasma-sprayed CrMnFeCoNi high entropy alloy coating, Mater. Des. 182 (2019) 108040, https://doi.org/10.1016/j.matdes.2019.108040.

[18] D.I. Proskurovsky, V.P. Rotshtein, G.E. Ozur, Y.F. Ivanov, A.B. Markov, Physical foundations for surface treatment of materials with low energy, high current electron beams, Surf. Coat. Tech. 125 (2000) 49–56, https://doi.org/10.1016/s0257-8972(99)00604-0.

[19] H. Xia, C.L. Zhang, P. Lv, J. Cai, Y.X. Jin, Q.F. Guan, Surface alloying of aluminum with molybdenum by high-current pulsed electron beam, Nucl. Instrum. Meth. B. 416 (2018) 9–15, https://doi.org/10.1016/j.nimb.2017.11.028.

[20] L.J. Chai, Z.M. Zhou, Z.P. Xiao, J. Tu, Y.P. Wang, W.J. Huang, Evolution of surface microstructure of Cu-50Cr alloy treated by high current pulsed electron beam, Sci. China Technol. Sci. 58 (3) (2015) 462–469, https://doi.org/10.1007/s11431-015-5774-7.

[21] C.L. Zhang, Q. Gao, P. Lv, J. Cai, C.T. Peng, Y.X. Jin, Q.F. Guan, Surface modification of Cu-W powder metallurgical alloy induced by high-current pulsed electron beam, Powder Technol. 325 (2018) 340–346, https://doi.org/10.1016/j.powtec.2017.11.037.

[22] T. Grosdidier, J.X. Zou, B. Bolle, S.Z. Hao, C. Dong, Grain refinement, hardening and metastable phase formation by high current pulsed electron beam (HCPEB) treatment under heating and melting modes, J. Alloys Compd. 504 (2010) S508–S511, https://doi.org/10.1016/j.jallcom.2010.04.010.

[23] C.L. Zhang, J. Cai, P. Lv, Y.W. Zhang, H. Xia, Q.F. Guan, Surface microstructure and properties of Cu-C powder metallurgical alloy induced by high-current pulsed electron beam, J. Alloy. Compd. 697 (2017) 96–103, https://doi.org/10.1016/j.jallcom.2016.12.119.

[24] C.L. Zhang, P. Lv, J. Cai, C.T. Peng, Y.X. Jin, Q.F. Guan, The microstructure and properties of tungsten alloying layer on copper by high-current pulse electron beam, Appl. Surf. Sci. 422 (2017) 582–590, https://doi.org/10.1016/j.apsusc.2017.06.049.

[25] D.N. Lee, A model for development of orientation of vapour deposits, J. Mater. Sci. 24 (12) (1989) 4375–4378, https://doi.org/10.1007/bf00544515.

[26] Y. Qin, C. Dong, X.G. Wang, S.Z. Hao, A.M. Wu, J.X. Zou, Y. Liu, Temperature profile and crater formation induced in high-current pulsed electron beam processing, J. Vac. Sci. Technol. A. 21 (2003) 1934–1938, https://doi.org/10.1116/1.1619417.

[27] Y. Qin, J.X. Zou, C. Dong, X.G. Wang, A.M. Wu, Y. Liu, S.Z. Hao, Q.F. Guan, Temperature–stress fields and related phenomena induced by a high current pulsed electron beam, Nucl. Instrum Meth. B 225 (4) (2004) 544–554, https://doi.org/10.1016/j.nimb.2004.06.008.

[28] Y. Shen, Z.X. Guo, M. Zhang, Q.F. Guan, Y.X. Jin, Y.H. Liu, Effect of high current pulsed electron beam surface irradiation on the microstructure and electrochemical behavior of zircaloy-4, Nucl. Instrum. Meth. B 434 (2018) 81–87, https://doi.org/10.1016/j.nimb.2018.08.042.

[29] P. Lv, X. Sun, J. Cai, C.L. Zhang, X.L. Liu, Q.F. Guan, Microstructure and high temperature oxidation resistance of nickel based alloy GH4169 irradiated by high current pulsed electron beam, Surf. Coat. Tech. 309 (2017) 401–409, https://doi.org/10.1016/j.surfcoat.2016.11.041.

[30] Y. Shen, J. Cai, P. Lv, C.L. Zhang, W. Huang, Q.F. Guan, Microstructures and properties of zirconium-702 irradiated by high current pulsed electron beam, Nucl. Instrum. Meth. B 358 (2015) 151–159, https://doi.org/10.1016/j.nimb.2015.06.020.

[31] W.H. Liu, Z.P. Lu, J.Y. He, J.H. Luan, Z.J. Wang, B. Liu, Y. Liu, M.W. Chen, C.T. Liu, Ductile CoCrFeNiMox high entropy alloys strengthened by hard intermetallic phases, Acta Mater. 116 (2016) 332–342, https://doi.org/10.1016/j.actamat.2016.06.063.

[32] S.H. Dong, C.L. Zhang, L.Y. Zhang, J. Cai, P. Lv, Y.X. Jin, Q.F. Guan, Microstructure and properties of Cu-Cr powder metallurgical alloy induced by high-current pulsed electron beam, J. Alloys Compd. 755 (2018) 251–256, https://doi.org/10.1016/j.jallcom.2018.04.291.

[33] Y. Zhang, T.T. Zuo, Y.Q. Cheng, P.K. Liaw, High-entropy alloys with high saturation magnetization, electrical resistivity, and malleability, Sci. Rep. 3 (2013) 1455, https://doi.org/10.1038/srep014.

[34] Z.B. Cai, X.F. Cui, Z. Liu, Y. Li, M.L. Dong, G. Jin, Microstructure and wear resistance of laser cladded Ni-Cr-Co-Ti-V highentropy alloy coating after laser remelting processing, Opt. Laser Technol. 99 (2018) 276–281, https://doi.org/10.1016/j.optlastec.2017.09.012.

[35] J. Cai, P. Lv, C.L. Zhang, J. Wu, C. Li, Q.F. Guan, Microstructure and properties of low carbon steel after surface alloying induced by high current pulsed electron beam, Nucl. Instrum. Meth. B 410 (2017) 47–52, https://doi.org/10.1016/j.nimb.2017.08.007.

[36] Z.Q. Zhang, S.Z. Yang, P. Lv, Y. Li, X.T. Wang, X.L. Hou, Q.F. Guan, The microstructures and corrosion properties of polycrystalline copper induced by high-current pulsed electron beam, Appl. Surf. Sci. 294 (2014) 9–14, https://doi.org/10.1016/j.apsusc.2013.12.178.

[37] J.X. Zou, K.M. Zhang, S.Z. Hao, C. Dong, T. Grosdidier, Mechanisms of hardening, wear and corrosion improvement of 316 L stainless steel by low energy high current pulsed electron beam surface treatment, Thin Solid Films 519 (2010) 1404–1415, https://doi.org/10.1016/j.tsf.2010.09.022.

[38] S.Z. Hao, L.M. Zhao, Y.L. Zhang, H.H. Wang, Improving corrosion and wear resistance of FV520B steel by high current pulsed electron beam surface treatment, Nucl. Instrum. Meth. B 356 (2015) 12–16, https://doi.org/10.1016/j.nimb.2015.04.046.

[39] Y. Samih, G. Marcos, N. Stein, N. Allain, E. Fleury, C. Dong, T. Grosdidier, Microstructure modifications and associated hardness and corrosion improvements in the AISI 420 martensitic stainless steel treated by high current pulsed electron beam (HCPEB), Surf. Coat. Tech. 259 (2014) 737–745, https://doi.org/10.1016/j.surfcoat.2014.09.065.